# Generation and reactivity of putative support systems, Ce-Al neutral binary oxide nanoclusters: CO oxidation and C–H bond activation

Zhe-Chen Wang, Shi Yin, and Elliot R. Bernstein

Citation: The Journal of Chemical Physics **139**, 194313 (2013); doi: 10.1063/1.4830406
View online: http://dx.doi.org/10.1063/1.4830406
View Table of Contents: http://aip.scitation.org/toc/jcp/139/19
Published by the American Institute of Physics

# Generation and reactivity of putative support systems, Ce-Al neutral binary oxide nanoclusters: CO oxidation and C–H bond activation

Zhe-Chen Wang, Shi Yin, and Elliot R. Bernstein[a)]
*Department of Chemistry and NSF ERC for Extreme Ultraviolet Science and Technology, Colorado State University, Fort Collins, Colorado 80523, USA*

(Received 4 September 2013; accepted 30 October 2013; published online 21 November 2013)

Both ceria ($CeO_2$) and alumina ($Al_2O_3$) are very important catalyst support materials. Neutral binary oxide nanoclusters (NBONCs), $Ce_xAl_yO_z$, are generated and detected in the gas phase and their reactivity with carbon monoxide (CO) and butane ($C_4H_{10}$) is studied. The very active species $CeAlO_4^{\bullet}$ can react with CO and butane via O atom transfer (OAT) and H atom transfer (HAT), respectively. Other $Ce_xAl_yO_z$ NBONCs do not show reactivities toward CO and $C_4H_{10}$. The structures, as well as the reactivities, of $Ce_xAl_yO_z$ NBONCs are studied theoretically employing density functional theory (DFT) calculations. The ground state $CeAlO_4^{\bullet}$ NBONC possesses a kite-shaped structure with an $O_tCeO_bO_bAlO_t$ configuration ($O_t$, terminal oxygen; $O_b$, bridging oxygen). An unpaired electron is localized on the $O_t$ atom of the $AlO_t$ moiety rather than the $CeO_t$ moiety: this $O_t$ centered radical moiety plays a very important role for the reactivity of the $CeAlO_4^{\bullet}$ NBONC. The reactivities of $Ce_2O_4$, $CeAlO_4^{\bullet}$, and $Al_2O_4$ toward CO are compared, emphasizing the importance of a spin-localized terminal oxygen for these reactions. Intramolecular charge distributions do not appear to play a role in the reactivities of these neutral clusters, but could be important for charged isoelectronic BONCs. DFT studies show that the reaction of $CeAlO_4^{\bullet}$ with $C_4H_{10}$ to form the $CeAlO_4H{\bullet}C_4H_9^{\bullet}$ encounter complex is barrierless. While HAT processes have been previously characterized for cationic and anionic oxide clusters, the reported study is the first observation of a HAT process supported by a ground state neutral oxide cluster. Mechanisms for catalytic oxidation of CO over surfaces of $Al_xO_y/M_mO_n$ or $M_mO_n/Al_xO_y$ materials are proposed consistent with the presented experimental and theoretical results. © *2013 AIP Publishing LLC*. [http://dx.doi.org/10.1063/1.4830406]

## I. INTRODUCTION

Ceria ($CeO_2$) is one of the most abundant rare earth oxides, and has been extensively studied over the past decades.[1–4] Ceria is mostly used as a catalyst support material: it helps to improve mechanical and thermal stability, as well as activity and selectivity of transition, noble, and rare earth metal oxide catalysts.[2,5] For example, ceria containing catalysts have been used in "three-way" catalytic converters,[6,7] solid oxide fuel cells,[8–11] and water splitting processes for hydrogen production.[12–14] These catalysts exhibit electrical conductivity and induce the formation of small polarons on the surfaces.[15–18] Aluminum oxides are also often used as supporting materials: they serve as a catalyst support for many industrial catalysts, such as those used in hydrodesulfurization, as well as other applications.[19–22] $Al_2O_3$ is also one of the most active catalysts for D/H exchange in mixtures of $D_2/CH_4$ and $CH_4/CD_4$; various aspects of C–H bond activation processes have been extensively studied for $\gamma$-$Al_2O_3$.[23–26] Quite recently, the reactive sites of $\gamma$-$Al_2O_3$ have been identified in a combined experimental/computational study, which has found that the presence of a moderate coverage with water increases the number of reactive nonadjacent Al-O Lewis acid base pairs.[24,25]

More recent studies focus on preparing nanomaterials of ceria and alumina to improve catalytic performance by increasing the distribution of surface defects, vacancies, or "active sites."[27–35] New applications are being explored by employing nanotechnology; e.g., vacancy engineered ceria nanostructures for protection from radiation-induced cellular damage and the neuro-protection offered by the auto-catalytic ceria nanoparticles.[29,31,36] The concept of preparing nanomaterials is to increase the surface to volume ratio and thereby increase the "active sites"; however, existing information on the precise nature and detailed operation of the active sites is still rather limited for many catalytic systems, even on the nanoscale.[37–39]

Gas phase nanoclusters in an "isolated" environment are ideal model systems with which to simulate real surface reactions and to discover surface reaction mechanisms.[37,39,40] Many excellent studies have been reported in the last decade with regard to the structure and reactivities of gas phase cationic[37,38,41–63] and anionic[42,64–79] oxide nanoclusters. Recently, He *et al.* reported systematic studies on the reactions of $Ce_mO_{2m}^+$ and $Ce_nO_{2n+1}^-$ clusters with CO and small hydrocarbons: they found very significant and interesting size-dependent reactivities under near room-temperature condition.[80–82] The groups of Wang and Jarrold performed detailed spectroscopic studies on aluminum oxide clusters.[76,83–87] Rather interesting reactivity trends are reported by the Schwarz and Castleman groups for oxidation

a)Author to whom correspondence should be addressed. Electronic mail: erb@lamar.colostate.edu

 

reactions generated by $Al_2O_3^+$,[51,88,89] and methane activation by the oxygen-rich $Al_2O_7^+$ cluster suggests the importance and influence of chemically absorbed $O_2$ for the C–H bond activation reaction.[43] Other studies of gas phase cerium and aluminum oxide ionic clusters can be found in Refs. 90 and 91.

A number of studies of neutral oxide nanoclusters (NONCs) in both matrix[92–95] and in the gas phase[39,96–116] have also appeared. Employing neutral oxide nanoclusters for the study of catalytic processes is advantageous, as it minimizes the effect of cluster charge, which has been considered to be significant with regard to cluster reactivity.[50,117,118] On the other hand, NONCs often have high vertical ionization energies (>8 eV) and multiphoton ionization with a 10 ns $Nd^{+3}$/YAG laser pulse can cause significant cluster fragmentation so as to confuse the mass spectra for reactant and product identification.[115,119] Recently, our group has developed a novel 118 nm, single-photon ionization (SPI) technique, which has proved to be reliable for detecting the distribution and reactivity of NONCs without dissociation.[112,116] Many gas phase NONCs and their reactivities have been studied in recent years (e.g., reactions of vanadium, cobalt, iron, manganese, and tantalum containing NONCs with CO,[100,105] ethene,[104,108] propene,[104,106] ethyne,[108] butane,[97] sulfur dioxide,[107] ammonia,[99,102] and methanol[103]). These cluster studies yield an understanding of the corresponding real catalytic systems and enable one to propose a full catalytic cycle at the molecular level for the bulk catalytic system.

In the last few years, the study of binary oxide nanoclusters (BONCs) has been reported for ionic systems. These cluster systems can serve as a more detailed molecular approach for the understanding of the active sites in catalytic supports and modified catalytic systems.[46,48,49,65,117,120–126] The first example of generating, as well as studying, the reactivity of BONCs is reported by He and co-workers: they proposed that the novel $AlVO_4^+$ cluster can activate $CH_4$ oxidation at room temperature.[49] Additionally, Schwarz and co-workers and He and co-workers report that $CH_4$ is activated by $V_3PO_{10}^+$.[121,124] The Schwarz group also illustrated the first complete gas phase catalytic cycle conducted by the $AlVO_3^+/AlVO_4^+$ BONC couple through both experimental and theoretical studies.[48] Sauer, Asmis, and co-workers studied the infrared spectroscopy of $CeVO_4^+$, $CeV_2O_6^+$, and $Ce_2VO_5^+$ BONCs for the first time, indicating interesting structures parallel to the condensed phase $VO_x/CeO_2$ supported materials.[46] They also reported enhanced $SO_2$ chemical absorption abilities via doping $V_4O_{10}^-$ cluster with Ti: the enhanced reactivity of $V_3TiO_{10}^-$ is attributed to charge localization on the outer oxygen atom that binds with the titanium atom. The presence of a free Ti-$O_t^\bullet$ ($O_t$: terminal oxygen) radical in $V_2Ti_2O_{10}^-$ allows binding of a second $SO_2$.[127] The initial studies of the photoelectron spectroscopy of anionic BONCs are reported by Jarrold and coworkers, whose group investigated the electronic structures of the $MoWO_y^-$ BONCs as well as other Mo or Al related BONCs.[128–135] Zheng *et al.* reported the photoelectron spectroscopy of $MAlO_x^-$ and $M_xAlO_2^-$ (M = Ti or V; $x$ = 1, 2, or 3) BONCs.[65,125] Studies of BONC ions are becoming increasingly widespread: e.g., $AuNbO_3^+$,[136] $V_xAg_yO_z^+$ ($x$ = 1–4, $y$ = 1–4, $z$ = 3–11),[137] $Al_xV_yO_z^-$,[123] $V_xY_yO_z^+$,[50,117] $V_xP_yO_z^+$,[138–140] and $AlYO_3^+$.[89,141] All the above systems are charged BONCs. Our group has extended BONC studies to neutral systems: in particular, neutral $V_xCo_yO_z$ BONCs are generated in the gas phase and their reactivity toward CO is determined.[100]

Both ceria and alumina are very important catalyst support materials. The gas-phase *ionic* Ce- or Al-relating oxide nanoclusters have been extensively studied. In the current work, we generate and detect $Ce_xAl_yO_z$ *neutral* binary oxide nanoclusters (NBONCs) in the gas phase, and explored their reactivity with CO and butane. The very active NBONC species $CeAlO_4^\bullet$ can react with CO and butane via O atom transfer (OAT) and H atom transfer (HAT) reactions, respectively. Structures, as well as the reactivities, of the $Ce_xAl_yO_z$ NBONCs are studied theoretically employing density functional theory (DFT) calculations. The influence of spin distribution and charge effect is considered for the reactivities. An ideal reaction mechanism on the solid surface of supported (e.g., $CeO_2$) aluminum oxide, and aluminum oxide containing other oxide catalytic materials, is proposed according to the presented experimental and theoretical results.

## II. EXPERIMENTAL AND THEORETICAL METHODS

The experimental setup for laser ablation coupled with a fast flow reactor employed in this work has been described previously in detail:[99,101–106,108,114,116,142,143] only a brief outline of the apparatus is given below. $Ce_xAl_yO_z$ clusters are generated by laser ablation of either a mixed metal target in the presence of ~1% $O_2$ seeded in a pure helium carrier gas (99.99%, General Air). The target is a pressed mixture of Ce (99%, Sigma Aldrich) and Al (99.0+%, Sigma Aldrich) powders (molar ratio = 1:1). A 10 Hz, focused, 532 nm $Nd^{3+}$:YAG laser ($Nd^{3+}$: yttrium aluminum garnet) with 10 mJ/pulse energy is used for the laser ablation. The expansion gas is pulsed into the vacuum by a supersonic nozzle (R. M. Jordan, Co.) with a backing pressure of typically 75 psi. Generated oxide clusters react with reactants in a fast flow reactor, which is directly coupled to the cluster generation channel. The reactant gases, CO (99.9% Sigma Aldrich), butane (99.0% Sigma Aldrich), and D-labeled butane ($C_4D_{10}$, 99.0% Sigma Aldrich) are used as purchased, at a 15 psi backing pressure, and injected into the reactor by a pulsed General Valve (Parker, Serial 9). The reactants and products are estimated to be thermalized to 300–400 K by collisions in the generation channel and the reaction cell. An electric field is placed downstream of the reactor in order to remove any residual ions from the molecular beam. The beam of neutral reactants and products is skimmed into a differentially pumped chamber and ionized by a separated VUV laser beam (118 nm, 10.5 eV/photon). The 118 nm laser light is generated by focusing the third harmonic (355 nm, ~30 mJ) of a $Nd^{3+}$:YAG laser in a tripling cell that contains about a 250 Torr argon/xenon (10/1) gas mixture. A $MgF_2$ prism (Crystaltechno LTD, Russia, 6° apex angle) is placed in the laser beam to enhance separation of the generated 118 nm laser beam from the defocused 355 nm input laser beam.

After the near threshold ionization, photoions are detected by a time of flight mass spectrometer (TOFMS).

DFT calculations are done using the Gaussian 09 program,[144] employing the hybrid B3LYP exchange-correlation functional[145–147] with the unrestricted Kohn–Sham solution.[148] The triple-zeta basis sets with Stuttgart/Dresden relativistic effective core potentials, 28 electrons in the core, denoted as SDD[149–152] in Gaussian 09 are adopted for Ce and the TZVP basis sets[153] for other atoms. For the optimization of transition structures (TS), we employed either the Berny algorithm[154] or the synchronous transit guided quasi-Newton (STQN) method.[155] For most cases, initial approximate structures of the transition structures are obtained by relaxed potential energy surface (PES) scans using an appropriate internal coordinate. Vibrational frequencies are calculated to characterize the nature of the stationary points as minima or transition structures; the relative energies (given in eV) are corrected for zero point energy (ZPE) contributions. Intrinsic reaction coordinate (IRC) calculations[156–158] are also performed to connect transition states (TS) with local minima. Test calculations indicate that basis set superposition error (BSSE) is negligible for these systems and thus it is not taken into account in this study.

## III. RESULTS AND DISCUSSION

Figure 1 shows the distribution of Ce-Al NBONCs within the mass range of 150 < m/z < 670, detected by 118 nm SPI time of flight mass spectrometry (TOFMS). The distribution is generated by laser ablation of a pressed Ce/Al metal disk with 0.5% $O_2$ seeded in helium carrier gas. The series $Ce_xAl_yO_z$ (e.g., $CeAlO_{3\text{-}5}$, $CeAl_2O_{4\text{-}6}$, $CeAl_3O_6$, $Ce_2AlO_{5,7}$, $Ce_2Al_2O_{6,7}$, $Ce_2Al_3O_{7,8}$, $Ce_2Al_4O_{10}$, and $Ce_2Al_5O_9$) can be observed. The efficiencies of ionization for observed clusters under 118 nm VUV laser are estimated to be roughly the same.

The reaction of Ce-Al NBONCs with CO is shown in Figure 2. The intensity of the signal for $CeAlO_4^\bullet$ decreases

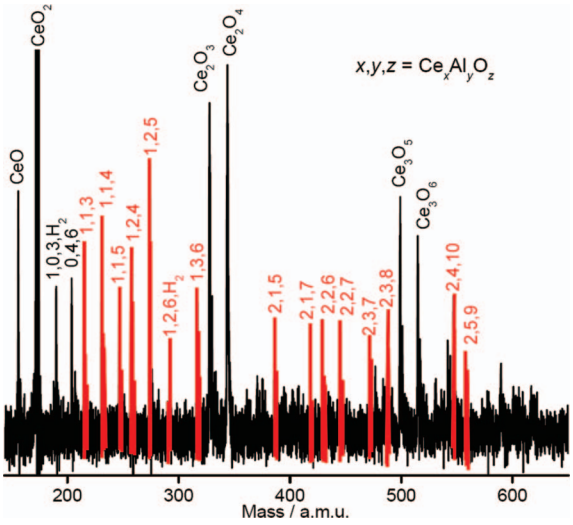


FIG. 1. Distribution of neutral Ce-Al BONCs (in red) detected by 118 nm SPI TOFMS, and $x,y,z = Ce_xAl_yO_z$.

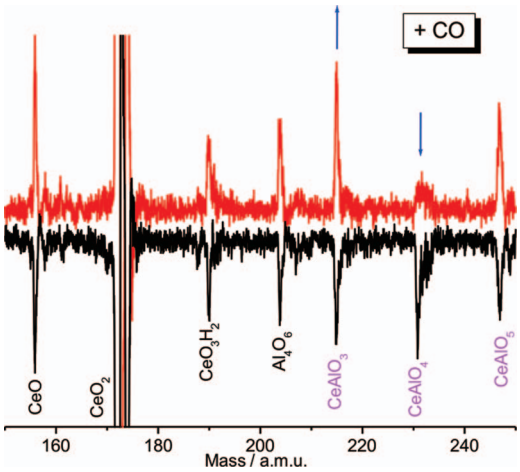


FIG. 2. Reaction of Ce-Al NBONCs with 4.2 Pa pure CO. The blue arrows point out the decrease of the $CeAlO_4^\bullet$ signal and the corresponding increase of the $CeAlO_3$ signal when CO is added to the reaction cell. The black trace on the lower panel is the distribution without CO. The decrease of $CeAlO_4^\bullet$ and the increase of $CeAlO_3^\bullet$ are roughly the same.

and that for $CeAlO_3^\bullet$ increases, if CO is added to the fast flow reaction cell, due to the reaction

$$CeAlO_4^\bullet + CO \rightarrow CeAlO_3^\bullet + CO_2 \; \Delta E = -1.35\,eV. \quad (1)$$

This reaction is exothermic according to DFT calculations ($\Delta E$, zero-point energy corrected reaction enthalpy at 0 K). The first order rate constant ($k$) in the fast flow reactor can be estimated by using the following equation:[49,105]

$$I = I_0 \exp(-k\rho l/v), \quad (2)$$

in which $I$ and $I_o$ are signal magnitudes for the clusters in the presence and absence of reactant gas, respectively; $\rho$ is the molecular density of reactant gas; $l$ is the effective path length of the reactor; and $v$ is the cluster beam velocity. The estimated rate constant for reaction (1) is on the order of $10^{-11}$ $cm^3$ $molecule^{-1}$ $s^{-1}$ according to our experimental results, with the estimated reaction-collisional efficiency of 4% (±50% uncertainty).

The other nanoclusters, such as homonuclear CeO, $CeO_2$, $Ce_2O_4$, $Al_4O_6$ or heteronuclear NBONCs, such as $CeAlO_{3,5}$, do not show evidence reactions with CO, which means that their reaction rate constants are lower than the observation limit of $10^{-13}$ $cm^3$ $molecule^{-1}$ $s^{-1}$. As for most catalysts, only certain localized sites (often thought as defects in surface structure) are considered to be active catalytic species. We proffer that $CeAlO_4$ is one such site, if not the only one: while others may exist, they are not amongst the observed unreactive species found in these experiments. Active catalytic surface sites should have structures, both electronic and geometric, similar to that found for $CeAlO_4$.

Figure 3 shows the generation and reaction of gas phase Ce-Al NBONCs with butane ($C_4H_{10}$) and D-labeled butane ($C_4D_{10}$). Of the clusters generated employing a Ce/Al mixed target, again $CeAlO_4^\bullet$ is the only species observed to react with $C_4H_{10}$ to generate the HAT products $CeAlO_4H$ and $C_4H_9^\bullet$ (Figure 3(b)),

$$CeAlO_4^\bullet + C_4H_{10} \rightarrow CeAlO_4H + C_4H_9^\bullet. \quad (3)$$

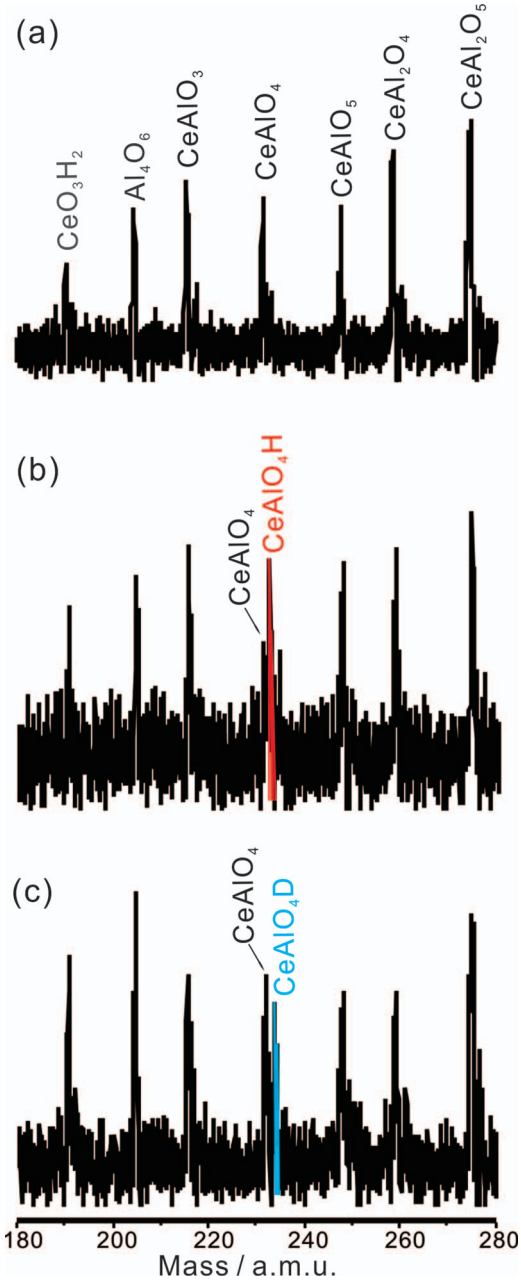


FIG. 3. Generation (a) and reaction of gas phase Ce-Al neutral BONCs with butane ($C_4H_{10}$) and D-labeled butane ($C_4D_{10}$) at the pressure of 5.9 Pa ((b) and (c)), respectively. A Ce-Al mixed target is employed for the experiments. The fluctuation of signal intense does not affect the observed reaction, since new product signals can be observed unambiguously.

Reaction (3) is further demonstrated if $C_4D_{10}$ is employed for the reaction, in which case the product $CeAlO_4D$ is observed (Figure 3(c)). The mass spectrum is very sensitive to experimental conditions, and the three spectra in Figure 3 are recorded at well controlled "identical" conditions except for the introduction of reactant gas for the lower two spectra. The experimental results shown in Figure 3 are highly repeatable. A HAT product is not observed for $CH_4$ or $C_2H_6$ introduced into the reaction cell as the reactant gas.

DFT optimized low energy isomers of $CeAlO_3^\bullet$ and $CeAlO_4^\bullet$ are shown in Figure 4. The diameters of the isomers are estimated to be around 0.5 nm. The lowest energy $CeAlO_3^\bullet$ (**1**) is in a doublet state with $C_s$ point group symmetry and a kite-shaped $O_tCe(O_b)_2Al$ structure ($O_t$, terminal oxygen; $O_b$, bridging oxygen). This structure is similar to that for neutral $V_2O_3$ or $CoVO_3^\bullet$ clusters,[100,109] substituting Al for V or Co at the two oxygen coordinated position and Ce for V at the three oxygen coordinated position, respectively. The $CeAlO_3^\bullet$ (**2**) isomer with the $Ce(O_b)_2AlO_t$ structure is only about 0.25 eV higher in energy. The energies of other $CeAlO_3^\bullet$ isomers are much higher than $O_tCe(O_b)_2Al^\bullet$ (**1**). For example, the energies of $O_tCeO_bAlO_t^\bullet$ (**3**) and $Ce(O_b)_3Al^\bullet$ (**4**) isomers are 0.85 and 0.92 eV higher than ground state structure, respectively (see Figure 4 for details). Among isomers of $CeAlO_4^\bullet$, the one with one Ce = $O_t$ and one Al–$O_t^\bullet$ terminal bond is identified to be the ground state $CeAlO_4^\bullet$ (**5**). The energies of other $CeAlO_4^\bullet$ isomers are much higher than that of the ground state $CeAlO_4^\bullet$ (**5**). Note that the unpaired electron is localized not on the rare earth metal centered Ce = $O_t$, but on the main-group metal centered Al-$O_t^\bullet$ oxygen, as shown in Figure 5. Former studies of charged nanoclusters such as $VAlO_4^{+\bullet}$,[48,49] $ScAlO_3^{+\bullet}$,[89,141] and $VAlO_5^{-\bullet}$[123] show that the Al-$O_t^\bullet$ moiety can act as the active site in cationic or anionic BONCs containing transition metals. Here our DFT studies show that the Al-$O_t^\bullet$ moiety could also be the

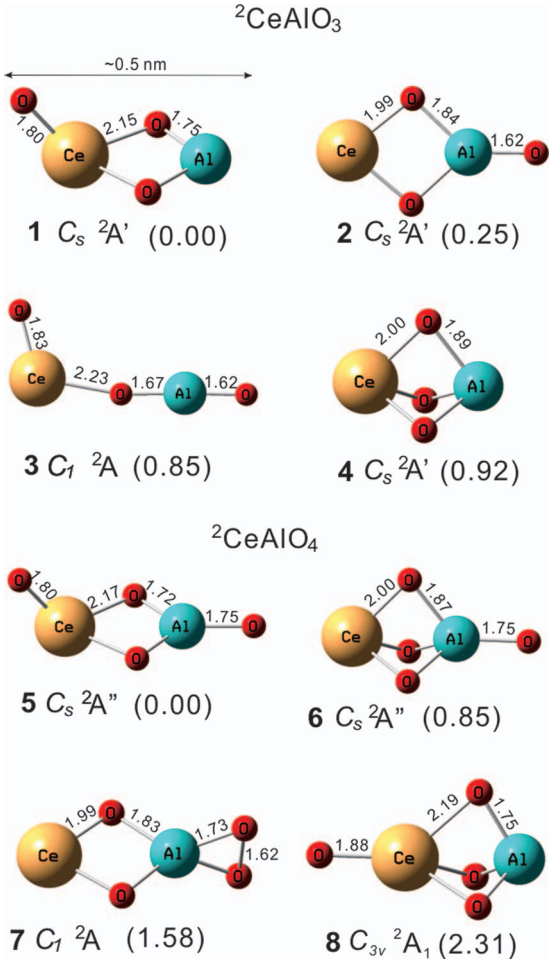


FIG. 4. Low-lying isomers of $CeAlO_3^\bullet$ and $CeAlO_4^\bullet$ NBONCs. The bond lengths are denoted in Å and the energies (in eV) are relative to the ground state and are zero point corrected.

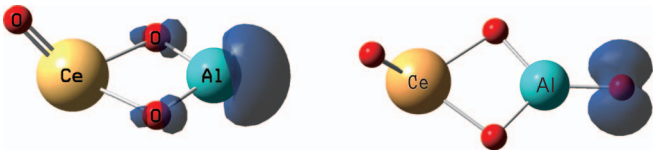


FIG. 5. Spin distribution for the NBONCs $CeAlO_3^\bullet$ and $CeAlO_4^\bullet$.

functional site in neutral nanoclusters such as $CeAlO_4^\bullet$. This result is in contrast with the traditional concept that both ceria and alumina are mainly used as non-active "supports" for the real catalytic transition metal species.

Ground state $CeAlO_4^\bullet$ possesses an unpaired electron spin localized at the terminal Al-$O_t^\bullet$ oxygen moiety (Figure 5). DFT calculations are performed for the ion/molecule reactions of $CeAlO_4^\bullet$ with $C_4H_{10}$ on the doublet ground state potential energy surface (PES). Figure 6 shows that the approaching of $C_4H_{10}$ to the $O_t^\bullet$ site of the Al-$O_t^\bullet$ moiety in $CeAlO_4^\bullet$ leads to the smooth HAT associated with a significant gain of energy (−1.13 eV). The DFT optimization process shows direct formation of the intermediate $CeAlO_4H\bullet C_4H_9^\bullet$ (**10**), which suggests that the key HAT steps in this reaction proceeds without a noticeable reaction barrier.

The reaction of $CeAlO_4^\bullet$ with CO is also studied employing DFT calculations. Reaction (1) involves an OAT from $CeAlO_4^\bullet$ to CO. The calculated potential energy surface for this process, as shown in Figure 7(b), reveals that the favorable oxidation proceeds by an initial bonding of the carbon atom of CO on the Al side of the $O_bO_bAlO_t^\bullet$ moiety to form the $O_tCe(O_b)_2Al(CO)O_t^\bullet$ encounter complex, intermediate **17**. Al binding to the C atom of CO rather than the O atom is typically rationalized by a mechanism that suggests electron donation from the HOMO of CO ($\sigma^*$) to an empty metal *d* orbital of Al and electron back donation from the filled metal d orbital of Al to the CO ($\pi^*$) LUMO. The initial process releases 0.59 eV binding energy, which provides enough energy for the following process of $CO_2$ moiety formation (**17** → **17/18** → **18**). Next the C-atom attacks the $O_t^\bullet$ atom of the $(O_b)_2AlO_t^\bullet$ moiety (transition state **17/18**, −0.25 eV), resulting in a rather stable intermediate **18** (−1.68 eV) with a nonlinear $CO_2$ moiety. The elongation of Al–O bond takes place easily to form the finally products $CO_2$ and

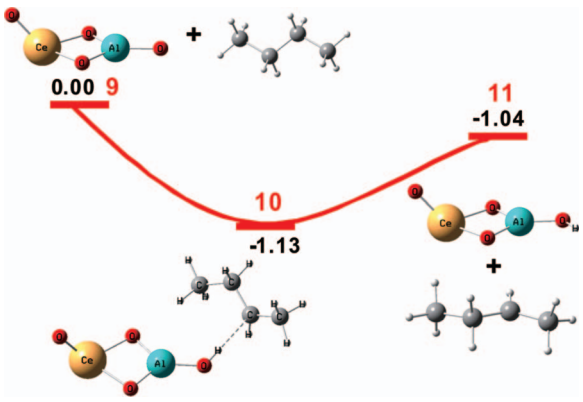


FIG. 6. Potential energy surfaces for the reactions of $C_4H_{10}$ with $CeAlO_4$. The red numbers (9, 10, 11) stand for reactants, intermediates, or products.

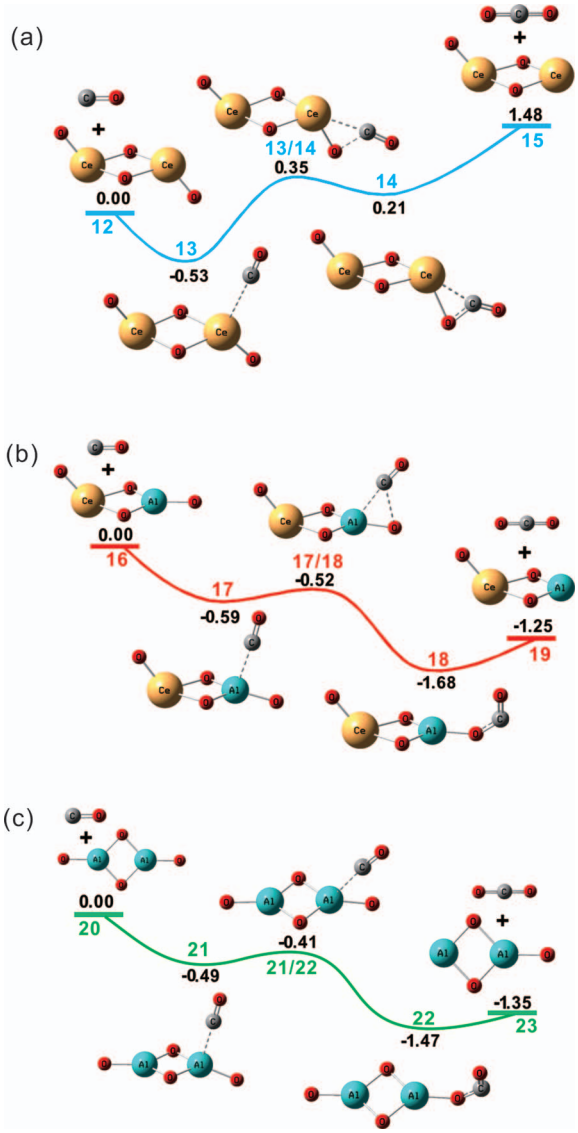


FIG. 7. DFT calculated potential energy surfaces for the reactions of CO with (a) $Ce_2O_4$, (b) $CeAlO_4^\bullet$, and (c) $Al_2O_4$, respectively. The red and green numbers *M* stand for reactants, intermediates, or products, and $M_1/M_2$ stand for transition states between intermediates $M_1$ and $M_2$.

$CeAlO_3^\bullet$. Note that the nonlinear $CO_2$ unit is fully located at the Al site rather than the Ce site in intermediate **18**.

For comparison, reactions of the homonuclear neutral clusters $Ce_2O_4$ and $Al_2O_4$ with CO are also studied employing the DFT calculation (Figures 7(a) and 7(c)), at the same level. The ground state of the neutral $Ce_2O_4$ is a closed-shell singlet $O_tCe(O_b)_2CeO_t$ structure without an unpaired, unequal spin distribution of the mixed clusters. The reaction of $Ce_2O_4$ with CO is endothermic

$$Ce_2O_4 + CO \rightarrow Ce_2O_3 + CO_2 \ \Delta E = 1.48\,eV. \qquad (4)$$

The approaching of CO to the Ce site of the $Ce_2O_4$ cluster leads to the formation of the $O_tCe(O_b)_2Ce(CO)O_t$ (**13**) encounter complex. The energy gained by forming the intermediate **13** (−0.53 eV) from the entrance channel of reaction (4) is similar to that for forming the intermediate $O_tCe(O_b)_2Al(CO)O_t$ (**17**, −0.59 eV) from reaction (1); however, a barrier (transition state **13/14**, 0.35 eV) occurs as the

C atom of the CO moiety attacks the $O_t$ atom of the $CeO_t$ moiety on the same site or side of the $Ce_2O_4(CO)$ cluster. The intermediate $O_tCe(O_b)_2CeCO_2$ (**14**) is formed from the transition state **13/14**. The energy of **14** is 0.21 eV higher than that of the $Ce_2O_4$ + CO entrance channel. The dissociation of the $CO_2$ moiety from **14** leads to the formation of the products $Ce_2O_3$ + $CO_2$. Comparing the reaction PESs of Figures 7(a) with 7(b), one can easily find that the large differences start from the C atom of the CO attacking the $O_t$ atom of the $(O_b)_2MO_t$ (M = Al or Ce) moieties. With the unpaired electron (spin) density localized on the $O_t^{\bullet}$ atom, interaction of the C atom with the $O_t$ atom to form the $CO_2$ moiety requires very little energy (Figure 7(b), **17** → **17/18**, the energy difference is only 0.07 eV). On the other hand, with no unpaired electron (spin) density involved in the interaction, the required energy for the CO bond formation can increase to as much as 0.88 eV for the barrier to form a $CO_2$ moiety (Figure 7(a), **13** → **13/14**).

The importance of spin localized terminal oxygen for this kind of reaction is further elucidated for homonuclear $Al_2O_4$ as the reactant to interact with CO,

$$Al_2O_4 + CO \rightarrow Al_2O_3 + CO_2\ \Delta E = -1.35\,eV. \quad (5)$$

According to DFT calculations, the ground state $Al_2O_4$ has a triplet diradical electronic distribution with a kite-shaped structure, in agreement with former experimental and theoretical studies.[159] The Mulliken atomic spin distribution (MASD) indicates that the two unpaired electrons are located on the two terminal oxygens of the neutral $Al_2O_4$ cluster. Figure 7(c) shows that the reaction of $Al_2O_4$ with CO is similar to that for $CeAlO_4^{\bullet}$ with CO, emphasizing the dominant role of the spin localized $O_t^{\bullet}$ as the active site.

The above discussion of electron distribution makes clear that the unpaired electron density on the terminal Al – attached O atom, $O_t$, plays a major role in the active site for OAT and HAT reactions for both $CeAlO_4^{\bullet}$ and $Al_2O_4$ NBONC. Additionally, however, we have noted that charged BONCs can also be active for such reactions, as well. One can also explore the affect of internal charge distribution on the OAT and HAT reactivity of neutral and charged BONCs: even for the cationic nanoclusters, the partial electrostatic charge difference can affect the reactivities.[50,160,161] The MASD as well as the electrostatic potential (ESP) distributions of $Ce_2O_4$, $CeAlO_4^{\bullet}$, and $Al_2O_4$ are shown in Figure 8. ESP distributions for these three clusters are very similar, which emphasizes once again that the spin localized $O_t^{\bullet}$ dominates the reaction of these three clusters for OAT and HAT reactions.

Charged clusters have also demonstrated activity with regard to OAT and HAT reactions. An isoelectronic system containing three nanoclusters with different charge states can be constructed and explored by similar DFT calculations: three such clusters are cationic $VAlO_4^{+\bullet}$, neutral $TiAlO_4^{\bullet}$, and anionic $ScAlO_4^{-\bullet}$ (see Figure 9).

The ground states of these three clusters possess the similar $(O_b)_2AlO_t^{\bullet}$ moieties as that of the neutral $CeAlO_4^{\bullet}$ nanocluster, while their ESP distributions are significantly different (see Figure 9 for details). The reactivity of cationic $VAlO_4^{+\bullet}$ has been studied previously by both experimental and theoretical studies.[48,49] Methane activation can be achieved by $VAlO_4^{+\bullet}$ at room temperature and a HAT process shows no observable barrier.[49] The nanocluster $VAlO_4^{+\bullet}$ is also very reactive toward CO.[48] The spin and electrostatic charge distributions of neutral $TiAlO_4^{\bullet}$ on the $(O_b)_2AlO_t^{\bullet}$ moiety are similar to those of NBONC $CeAlO_4^{\bullet}$: the latter reacts with $C_4H_{10}$ via HAT but does not react with $CH_4$. The ground state structure of $ScAlO_4^{-\bullet}$ is similar to that of

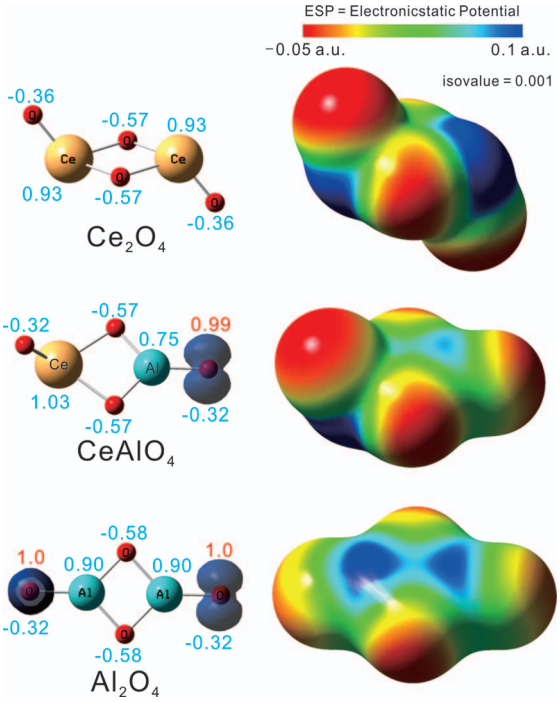


FIG. 8. Charge and spin distributions of neutral nanoclusters $Ce_2O_4$, $CeAlO_4^{\bullet}$, and $Al_2O_4$. The Mulliken atomic charge values are denoted in blue and the Mulliken atomic spins distributions are denoted in red, on the structures at the left.

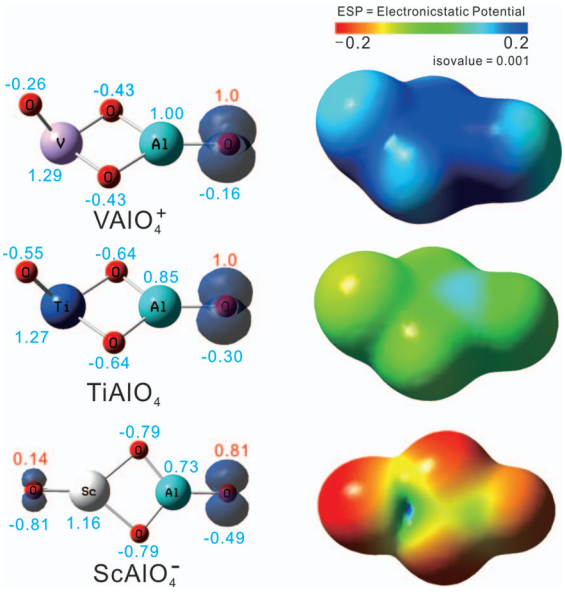


FIG. 9. Charge and spin distributions of isoelectronic nanoclusters $VAlO_4^{+\bullet}$, $TiAlO_4^{\bullet}$, and $ScAlO_4^{-\bullet}$. The Mulliken atomic charge values are denoted in blue color and the Mulliken atomic spins distributions are denoted in red color, on the structures at the left.

$Al_2O_4^{-\bullet}$, which is covalently isoelectronic to $ScAlO_4^{-\bullet}$. Further, recent studies show that $Al_2O_4^{-\bullet}$ is an active species since it can react with both CO and $C_4H_{10}$.[88,162] The reactions of methane with $VAlO_4^{+\bullet}$, $TiAlO_4^{\bullet}$, and $ScAlO_4^{-\bullet}$ are selected as a typical comparison system for elucidating the charge effect (Figure 10) on the reactivity of these clusters. All three reactions are exothermic:

$$VAlO_4^{+\bullet} + CH_4 \rightarrow VAlO_4H^+ + CH_3^{\bullet}\ \Delta E = -1.10\,eV, \quad (6)$$

$$TiAlO_4^{\bullet} + CH_4 \rightarrow TiAlO_4H + CH_3^{\bullet}\ \Delta E = -0.74\,eV, \quad (7)$$

$$ScAlO_4^{-\bullet} + CH_4 \rightarrow ScAlO_4H^- + CH_3^{\bullet}\ \Delta E = -0.34\,eV. \quad (8)$$

Reaction (6) is barrierless even at room temperature and the formation of the $VAlO_4H^+{\bullet}CH_3^{\bullet}$ (**26**) intermediate is straightforward without any barrier (Figure 10(a)). The encounter complex $VAlO_4^{+}{\bullet}CH_4^{\bullet}$ (**25**) and the following transition state $VAlO_4^{+}{\bullet}H{\bullet}CH_3^{\bullet}$ (**25/26**) cannot be located.[49] Unlike the cationic reaction (6), that the encounter complex for neutral reaction (7), $TiAlO_4{\bullet}CH_4^{\bullet}$ (**29**), is easily located and the transition state $TiAlO_4{\bullet}H{\bullet}CH_3^{\bullet}$ (**29/30**) between $TiAlO_4{\bullet}CH_4^{\bullet}$ (**29**) and $TiAlO_4H{\bullet}CH_3^{\bullet}$ (**30**) can also be fully optimized (Figure 10(b)). Although the ZPE corrected energy of transition state **26/27** (−0.06 eV) is slightly lower than the entrance channel, taking entropy into consideration, according to a Gibbs free energy calculation, reaction (7) is not favorable at room temperature. The HAT transition state $ScAlO_4^{-}{\bullet}H{\bullet}CH_3^{\bullet}$ (**33/34**) is the key species in the anionic reaction (8), showing clearly a barrier (0.18 eV) for this anionic reaction (Figure 10(c)). Comparison of reaction (6)–(8) suggests that for a certain structure with identified spin distribution, electrostatic charge modification may be an effective way to adjust the reactivity and selectivity of some catalytic reactions, even though the reaction site is still clearly the Al-$O_t^{\bullet}$ moiety of the BONCs.

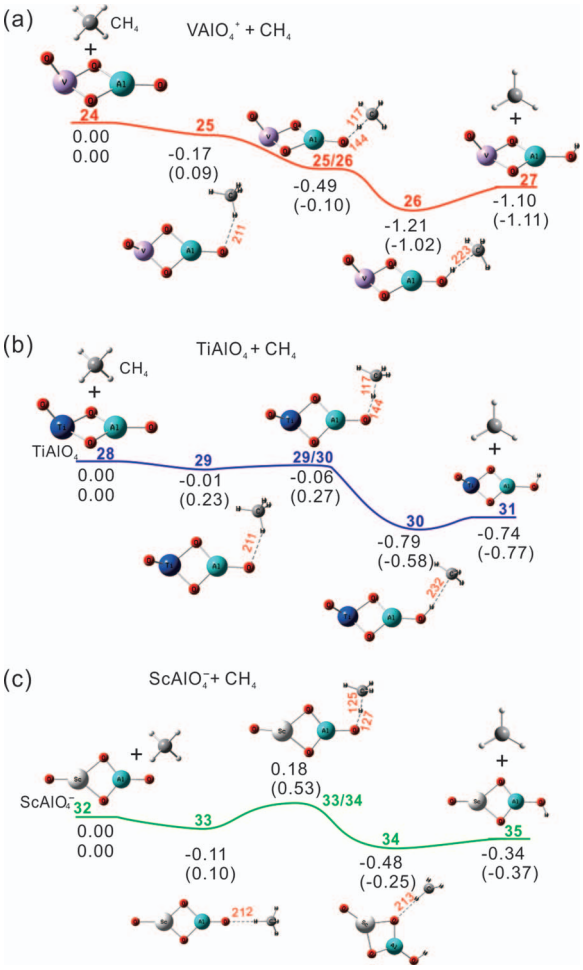


FIG. 10. The PESs for reactions of methane with (a) $VAlO_4^{+\bullet}$, (b) $TiAlO_4^{\bullet}$, and (c) $ScAlO_4^{-\bullet}$. The key bond lengths are denoted in Å. The zero-point corrected energy and Gibbs free energies (in the parentheses) are denoted in eV. The number $M$ stands for the intermediates while $M_1/M_2$ stands for the transition state between intermediates $M_1$ and $M_2$. Note that **25** and **25/26** are obtained by fixing the OH bond (2.11 Å) or O–H and H–C bonds (1.44 and 1.17 Å), respectively, and at the same time relaxing all the other reaction coordinates. The intermediate $O_tV(O_b)_2AlO_t{\bullet}HCH_3^{\bullet}$ (similar to **25**) in (a) cannot be located.

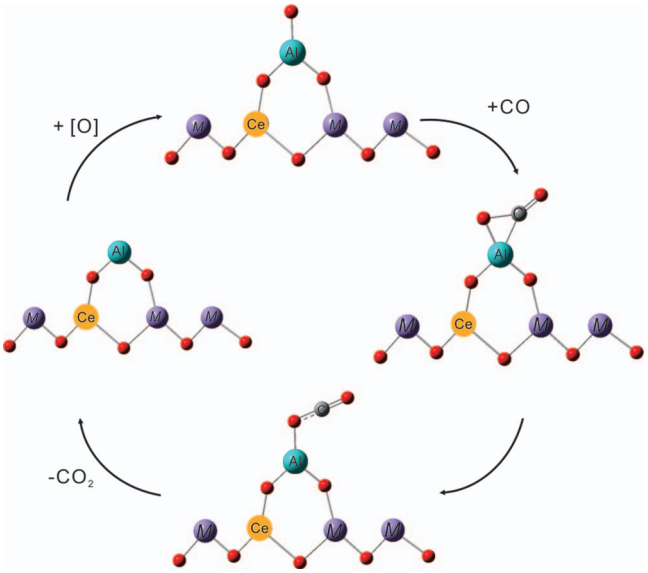


FIG. 11. Schematic diagram for the catalytic oxidation reactions of CO on the surfaces of $Ce_mO_n/Al_xO_y$ supporting system is shown. (M: Al, Ce, or other main-group or transition metals, purple colored.)

The gas phase nanocluster $CeAlO_4$ provides a clear and perhaps ideal mechanism for the CO oxidation by a real Ce-Al oxide surface (see Figure 11(a) for details): (1) CO is chemically absorbed on the Al site; (2) CO interacts with $O_t$ atoms bonding to the Al site, forming a nonlinear $CO_2$ unit; and (3) another O atom from $O_2$ or other oxidants can be added to Al site to complete the proposed catalytic cycle. This catalytic cycle suggests a mechanism for a Ce-Al oxide catalyst surface enhancing the CO to $CO_2$ oxidation reaction. Moreover, even taking alumina as a supporting material, the $(O_b)_2AlO_t$ moiety can still play the major role in catalytic reactions (Figure 11(b)). The "supported material" may just be added to "modify" the reactivity of the surface of alumina: this mechanism is not consistent with the traditional concepts that the supported materials are the active species and that the supporting material (such as alumina) is important only to enhance surface area and access, but is otherwise inert.

## IV. CONCLUSIONS

Neutral $Ce_xAl_yO_z$ nanoclusters are generated by laser ablation, and their reactions with CO and $C_4H_{10}$ are studied. The neutral bimetallic nanocluster $CeAlO_4^\bullet$ is highly reactive with CO ($CeAlO_4^\bullet + CO \rightarrow CeAlO_3^\bullet + CO_2$), while the pure $Ce_2O_4$ cluster is not. $CeAlO_4^\bullet$ can also perform C–H bond activation via reaction with $C_4H_{10}$ to produce $CeAlO_4H$ and $C_4H_9^\bullet$. DFT studies show that the spin localized terminal oxygen at the Al site instead of the Ce site plays a major role in these reactions. The charge distribution over clusters can also affect the reactivities, but are not the main driver of the O- or H-atom transfer reactions. The HAT process for the reaction of $CeAlO_4^\bullet$ with $C_4H_{10}$ is barrierless to form the $CeAlO_4H{\bullet}C_4H_9^\bullet$ encounter complex. This is the first observation of a HAT process supported by a ground state, neutral oxide cluster. Mechanisms for the catalytic oxidation of CO over surfaces of $Al_xO_y/Ce_mO_n$ or $Ce_mO_n/Al_xO_y$ materials are proposed based on these experimental and theoretical results. This research implies that the $Al_xO_y$ sites on "$Al_xO_y/Ce_mO_n$ supporting systems" can also be highly reactive. Supporting materials such as $Al_2O_3$ can be more functional and complex than has been traditionally conceived: they are apparently not simply "inert materials."

## ACKNOWLEDGMENTS

We thank the AFOSR (Grant No. FA9550-10-1-0454), the NSF ERC for EUV Science and Technology (Grant No. 0310717) and XSEDE supercomputer resources provided by SDSC (Grant No. TG-CHE110083) for support of this work.

[1] J. Paier, C. Penschke, and J. Sauer, Chem. Rev. **113**, 3949 (2013).
[2] Q. Fu, H. Saltsburg, and M. Flytzani-Stephanopoulos, Science **301**, 935 (2003).
[3] A. Trovarelli, Catal. Rev. - Sci. Eng. **38**, 439 (1996).
[4] H. C. Yao and Y. F. Y. Yao, J. Catal. **86**, 254 (1984).
[5] A. Gupta, U. V. Waghmare, and M. S. Hegde, Chem. Mater. **22**, 5184 (2010).
[6] J. Kaspar, P. Fornasiero, and M. Graziani, Catal. Today **50**, 285 (1999).
[7] A. Trovarelli, C. de Leitenburg, M. Boaro, and G. Dolcetti, Catal. Today **50**, 353 (1999).
[8] Z. P. Shao and S. M. Haile, Nature (London) **431**, 170 (2004).
[9] S. D. Park, J. M. Vohs, and R. J. Gorte, Nature (London) **404**, 265 (2000).
[10] M. Mogensen, N. M. Sammes, and G. A. Tompsett, Solid State Ionics **129**, 63 (2000).
[11] E. P. Murray, T. Tsai, and S. A. Barnett, Nature (London) **400**, 649 (1999).
[12] A. Primo, T. Marino, A. Corma, R. Molinari, and H. Garcia, J. Am. Chem. Soc. **133**, 6930 (2011).
[13] S. Abanades, A. Legal, A. Cordier, G. Peraudeau, G. Flamant, and A. Julbe, J. Mater. Sci. **45**, 4163 (2010).
[14] H. Kaneko, T. Miura, H. Ishihara, S. Taku, T. Yokoyama, H. Nakajima, and Y. Tamaura, Energy **32**, 656 (2007).
[15] S. Kim and J. Maier, J. Electrochem. Soc. **149**, J73 (2002).
[16] A. Tschope, E. Sommer, and R. Birringer, Solid State Ionics **139**, 255 (2001).
[17] S. R. Wang, T. Kobayashi, M. Dokiya, and T. Hashimoto, J. Electrochem. Soc. **147**, 3606 (2000).
[18] S. Lubke and H. D. Wiemhofer, Solid State Ionics **117**, 229 (1999).
[19] H. H. Brintzinger, D. Fischer, R. Mulhaupt, B. Rieger, and R. M. Waymouth, Angew. Chem., Int. Ed. **34**, 1143 (1995).
[20] L. Resconi, L. Cavallo, A. Fait, and F. Piemontesi, Chem. Rev. **100**, 1253 (2000).
[21] F. Bataille, J. L. Lemberton, P. Michaud, G. Perot, M. Vrinat, M. Lemaire, E. Schulz, M. Breysse, and S. Kasztelan, J. Catal. **191**, 409 (2000).
[22] A. N. Startsev, Catal. Rev. - Sci. Eng. **37**, 353 (1995).
[23] R. Wischert, P. Laurent, C. Coperet, F. Delbecq, and P. Sautet, J. Am. Chem. Soc. **134**, 14430 (2012).
[24] R. Wischert, C. Copéret, F. Delbecq, and P. Sautet, Angew. Chem. Int. Ed. **50**, 3202 (2011).
[25] C. Copeéret, Chem. Rev. **110**, 656 (2010).
[26] J. Joubert, A. Salameh, V. Krakoviack, F. Delbecq, P. Sautet, C. Copéret, and J. M. Basset, J. Phys. Chem. B **110**, 23944 (2006).
[27] C. Loschen, A. Migani, S. T. Bromley, F. Illas, and K. M. Neyman, Phys. Chem. Chem. Phys. **10**, 5730 (2008).
[28] M. Cargnello, N. L. Wieder, T. Montini, R. J. Gorte, and P. Fornasiero, J. Am. Chem. Soc. **132**, 1402 (2010).
[29] M. Das, S. Patil, N. Bhargava, J. F. Kang, L. M. Riedel, S. Seal, and J. J. Hickman, Biomaterials **28**, 1918 (2007).
[30] S. P. Jiang, Mater. Sci. Eng., A **418**, 199 (2006).
[31] R. W. Tarnuzzer, J. Colon, S. Patil, and S. Seal, Nano Lett. **5**, 2573 (2005).
[32] S. Tsunekawa, R. Sivamohan, S. Ito, A. Kasuya, and T. Fukuda, Nanostruct. Mater. **11**, 141 (1999).
[33] S. Z. Chu, K. Wada, S. Inoue, M. Isogai, and A. Yasumori, Adv. Mater. **17**, 2115 (2005).
[34] J. P. Zhang, Z. M. Fu, Z. X. Yang, and S. F. Li, Phys. Lett. A **376**, 3235 (2012).
[35] S. Mandal, K. K. Bando, C. Santra, S. Maity, O. O. James, D. Mehta, and B. Chowdhury, Appl. Catal. A **452**, 94 (2013).
[36] D. Schubert, R. Dargusch, J. Raitano, and S. W. Chan, Biochem. Biophys. Res. Commun. **342**, 86 (2006).
[37] H. Schwarz, Angew. Chem. Int. Ed. **50**, 10096 (2011).
[38] J. Roithová and D. Schröder, Chem. Rev. **110**, 1170 (2010).
[39] S. Yin and E. R. Bernstein, Int. J. Mass Spectrom. **321**, 49 (2012).
[40] S. J. Peppernick, K. D. D. Gunaratne, and A. W. Castleman, Jr., Proc. Natl. Acad. Sci. U.S.A. **107**, 975 (2010).
[41] D. K. Böhme and H. Schwarz, Angew. Chem. Int. Ed. **44**, 2336 (2005).
[42] H.-J. Zhai, X.-H. Zhang, W.-J. Chen, X. Huang, and L.-S. Wang, J. Am. Chem. Soc. **133**, 3085 (2011).
[43] Z.-C. Wang, T. Weiske, R. Kretschmer, M. Schlangen, M. Kaupp, and H. Schwarz, J. Am. Chem. Soc. **133**, 16930 (2011).
[44] A. M. Ricks, L. Gagliardi, and M. A. Duncan, J. Phys. Chem. Lett. **2**, 1662 (2011).
[45] K. Kwapien, M. Sierka, J. Dobler, J. Sauer, M. Haertelt, A. Fielicke, and G. Meijer, Angew. Chem. Int. Ed. **50**, 1716 (2011).
[46] L. Jiang, T. Wende, P. Claes, S. Bhattacharyya, M. Sierka, G. Meijer, P. Lievens, J. Sauer, and K. R. Asmis, J. Phys. Chem. A **115**, 11187 (2011).
[47] G. Santambrogio, E. Janssens, S. H. Li, T. Siebert, G. Meijer, K. R. Asmis, J. Dobler, M. Sierka, and J. Sauer, J. Am. Chem. Soc. **130**, 15143 (2008).
[48] Z.-C. Wang, N. Dietl, R. Kretschmer, T. Weiske, M. Schlangen, and H. Schwarz, Angew. Chem. Int. Ed. **50**, 12351 (2011).
[49] Z.-C. Wang, X.-N. Wu, Y.-X. Zhao, J.-B. Ma, X.-L. Ding, and S.-G. He, Chem. Phys. Lett. **489**, 25 (2010).
[50] X.-L. Ding, X.-N. Wu, Y.-X. Zhao, and S.-G. He, Acc. Chem. Res. **45**, 382 (2012).
[51] Z.-C. Wang, N. Dietl, R. Kretschmer, J.-B. Ma, T. Weiske, M. Schlangen, and H. Schwarz, Angew. Chem. Int. Ed. **51**, 3703 (2012).
[52] M. J. Y. Jarvis, V. Blagojevic, G. K. Koyanagi, and D. K. Bohme, J. Phys. Chem. A **117**, 1151 (2013).
[53] V. Blagojevic, M. J. Y. Jarvis, G. K. Koyanagi, and D. K. Bohme, J. Phys. Chem. A **117**, 3786 (2013).
[54] R. C. Dunbar, J. Oomens, G. Orlova, and D. K. Bohme, Int. J. Mass Spectrom. **308**, 330 (2011).
[55] G. K. Koyanagi, V. Kapishon, D. K. Bohme, X. H. Zhang, and H. Schwarz, Eur. J. Inorg. Chem. **2010**, 1516 (2010).
[56] M. J. Y. Jarvis, V. Blagojevic, G. K. Koyanagi, and D. K. Bohme, Phys. Chem. Chem. Phys. **12**, 4852 (2010).
[57] A. Bozovic, S. Feil, G. K. Koyanagi, A. A. Viggiano, X. H. Zhang, M. Schlangen, H. Schwarz, and D. K. Bohme, Chem. Eur. J. **16**, 11605 (2010).
[58] A. Shayesteh, V. V. Lavrov, G. K. Koyanagi, and D. K. Bohme, J. Phys. Chem. A **113**, 5602 (2009).
[59] X. Zhao, A. C. Hopkinson, and D. K. Bohme, Chem. Phys. Chem. **9**, 873 (2008).
[60] V. Blagojevic, A. Bozovic, G. Orlova, and D. K. Bohme, J. Phys. Chem. A **112**, 10141 (2008).
[61] J. L. Snow, G. Orlova, V. Blagojevic, and D. K. Bohme, J. Am. Chem. Soc. **129**, 9910 (2007).
[62] V. Blagojevic and D. K. Böhme, Int. J. Mass Spectrom. **254**, 152 (2006).

[63] V. Blagojevic, G. Orlova, and D. K. Böhme, J. Am. Chem. Soc. **127**, 3545 (2005).
[64] J. U. Reveles, G. E. Johnson, S. N. Khanna, and A. W. Castleman, Jr., J. Phys. Chem. C **114**, 5438 (2010).
[65] Z.-G. Zhang, H.-G. Xu, X.-Y. Kong, and W.-J. Zheng, J. Phys. Chem. A **115**, 13 (2011).
[66] S. G. Li, H. J. Zhai, L. S. Wang, and D. A. Dixon, J. Phys. Chem. A **113**, 11273 (2009).
[67] H. J. Zhai and L. S. Wang, J. Am. Chem. Soc. **129**, 3022 (2007).
[68] H. J. Zhai, J. Döbler, J. Sauer, and L. S. Wang, J. Am. Chem. Soc. **129**, 13270 (2007).
[69] H. J. Zhai and L. S. Wang, J. Chem. Phys. **125**, 164315 (2006).
[70] H. J. Zhai, W. J. Chen, X. Huang, and L. S. Wang, RSC Advances **2**, 2707 (2012).
[71] R. Pal, L. M. Wang, Y. Pei, L. S. Wang, and X. C. Zeng, J. Am. Chem. Soc. **134**, 9438 (2012).
[72] S. G. Li, H. J. Zhai, L. S. Wang, and D. A. Dixon, J. Phys. Chem. A **116**, 5256 (2012).
[73] W. Huang, H. J. Zhai, and L. S. Wang, J. Am. Chem. Soc. **132**, 4344 (2010).
[74] H. J. Zhai, B. Wang, X. Huang, and L. S. Wang, J. Phys. Chem. A **113**, 9804 (2009).
[75] H. J. Zhai, B. Wang, X. Huang, and L. S. Wang, J. Phys. Chem. A **113**, 3866 (2009).
[76] M. Sierka, J. Döbler, J. Sauer, H. J. Zhai, and L. S. Wang, Chem. Phys. Chem. **10**, 2410 (2009).
[77] H. J. Zhai, B. B. Averkiev, D. Y. Zubarev, L. S. Wang, and A. I. Boldyrev, Angew. Chem. Int. Ed. **46**, 4277 (2007).
[78] X. Huang, H. J. Zhai, T. Waters, J. Li, and L. S. Wang, Angew. Chem. Int. Ed. **45**, 657 (2006).
[79] X. Huang, H. J. Zhai, J. Li, and L. S. Wang, J. Phys. Chem. A **110**, 85 (2006).
[80] X. N. Wu, X. L. Ding, S. M. Bai, B. Xu, S. G. He, and Q. Shi, J. Phys. Chem. C **115**, 13329 (2011).
[81] X. L. Ding, X. N. Wu, Y. X. Zhao, J. B. Ma, and S. G. He, Chem. Phys. Chem. **12**, 2046 (2011).
[82] X. N. Wu, Y. X. Zhao, W. Xue, Z. C. Wang, S. G. He, and X. L. Ding, Phys. Chem. Chem. Phys. **12**, 3984 (2010).
[83] R. B. Wyrwas, C. C. Jarrold, U. Das, and K. Raghavachari, J. Chem. Phys. **124**, 201101 (2006).
[84] U. Das, K. Raghavachari, and C. C. Jarrold, J. Chem. Phys. **122**, 014313 (2005).
[85] F. A. Akin and C. C. Jarrold, J. Chem. Phys. **120**, 8698 (2004).
[86] F. A. Akin and C. C. Jarrold, J. Chem. Phys. **118**, 1773 (2003).
[87] F. A. Akin and C. C. Jarrold, J. Chem. Phys. **118**, 5841 (2003).
[88] G. E. Johnson, E. C. Tyo, and A. W. Castleman, Jr., J. Phys. Chem. A **112**, 4732 (2008).
[89] J. B. Ma, Z. C. Wang, M. Schlangen, S. G. He, and H. Schwarz, Angew. Chem. Int. Ed. **51**, 5991 (2012).
[90] P. Yang, J. H. Ge, and Z. Y. Jiang, Chin. Phys. **16**, 1014 (2007).
[91] A. B. C. Patzer, C. Chang, E. Sedlmayr, and D. Sulzle, Eur. Phys. J. D **32**, 329 (2005).
[92] J. Zhuang, Z. H. Li, K. N. A. Fan, and M. F. Zhou, J. Phys. Chem. A **116**, 3388 (2012).
[93] M. F. Zhou, J. Zhuang, Z. J. Zhou, Z. H. Li, Y. Y. Zhao, X. M. Zheng, and K. N. Fan, J. Phys. Chem. A **115**, 6551 (2011).
[94] M. F. Zhou, J. Zhuang, G. J. Wang, and M. H. Chen, J. Phys. Chem. A **115**, 2238 (2011).
[95] M. F. Zhou, Z. J. Zhou, J. Zhuang, Z. H. Li, K. N. Fan, Y. Y. Zhao, and X. M. Zheng, J. Phys. Chem. A **115**, 14361 (2011).
[96] S. Yin, Z. Wang, and E. R. Bernstein, Phys. Chem. Chem. Phys. **15**, 4699 (2013).
[97] Z.-C. Wang, S. Yin, and E. R. Bernstein, J. Phys. Chem. A **117**, 2294 (2013).
[98] Z. C. Wang, S. Yin, and E. R. Bernstein, Phys. Chem. Chem. Phys. **15**, 10429 (2013).
[99] S. Yin, Y. Xie, and E. R. Bernstein, J. Chem. Phys. **137**, 124304 (2012).
[100] Z.-C. Wang, S. Yin, and E. R. Bernstein, J. Phys. Chem. Lett. **3**, 2415 (2012).
[101] Y. Xie, F. Dong, S. Heinbuch, J. J. Rocca, and E. R. Bernstein, Phys. Chem. Chem. Phys. **12**, 947 (2010).
[102] S. Heinbuch, F. Dong, J. J. Rocca, and E. R. Bernstein, J. Chem. Phys. **133**, 174314 (2010).
[103] F. Dong, S. Heinbuch, Y. Xie, J. J. Rocca, and E. R. Bernstein, J. Phys. Chem. A **113**, 3029 (2009).
[104] F. Dong, S. Heinbuch, Y. Xie, E. R. Bernstein, J. J. Rocca, Z. C. Wang, X. L. Ding, and S. G. He, J. Am. Chem. Soc. **131**, 1057 (2009).
[105] W. Xue, Z.-C. Wang, S.-G. He, Y. Xie, and E. R. Bernstein, J. Am. Chem. Soc. **130**, 15879 (2008).
[106] Z.-C. Wang, W. Xue, Y.-P. Ma, X.-L. Ding, S.-G. He, F. Dong, S. Heinbuch, J. J. Rocca, and E. R. Bernstein, J. Phys. Chem. A **112**, 5984 (2008).
[107] S.-G. He, Y. Xie, F. Dong, S. Heinbuch, E. Jakubikova, J. J. Rocca, and E. R. Bernstein, J. Phys. Chem. A **112**, 11067 (2008).
[108] F. Dong, S. Heinbuch, Y. Xie, J. J. Rocca, E. R. Bernstein, Z.-C. Wang, K. Deng, and S.-G. He, J. Am. Chem. Soc. **130**, 1932 (2008).
[109] E. Jakubikova, A. K. Rappé, and E. R. Bernstein, J. Phys. Chem. A **111**, 12938 (2007).
[110] E. Jakubikova and E. R. Bernstein, J. Phys. Chem. A **111**, 13339 (2007).
[111] F. Dong, S. Heinbuch, S. G. He, Y. Xie, J. J. Rocca, and E. R. Bernstein, J. Chem. Phys. **125**, 164318 (2006).
[112] Y. Matsuda and E. R. Bernstein, J. Phys. Chem. A **109**, 3803 (2005).
[113] W. Kang and E. R. Bernstein, Bull. Korean Chem. Soc. **26**, 345 (2005).
[114] D. N. Shin, Y. Matsuda, and E. R. Bernstein, J. Chem. Phys. **120**, 4157 (2004).
[115] Y. Matsuda, D. N. Shin, and E. R. Bernstein, J. Chem. Phys. **120**, 4142 (2004).
[116] Y. Matsuda and E. R. Bernstein, J. Phys. Chem. A **109**, 314 (2005).
[117] Z.-Y. Li, Y.-X. Zhao, X.-N. Wu, X.-L. Ding, and S.-G. He, Chem. Eur. J. **17**, 11728 (2011).
[118] G. E. Johnson, R. Mitrić, M. Nössler, E. C. Tyo, V. Bonačić-Koutecký, and A. W. Castleman, Jr., J. Am. Chem. Soc. **131**, 5460 (2009).
[119] Y. Matsuda, D. N. Shin, and E. R. Bernstein, J. Chem. Phys. **120**, 4165 (2004).
[120] Y.-X. Zhao, X.-N. Wu, J.-B. Ma, S.-G. He, and X.-L. Ding, J. Phys. Chem. C **114**, 12271 (2010).
[121] J. B. Ma, X. N. Wu, Y. X. Zhao, X. L. Ding, and S. G. He, Phys. Chem. Chem. Phys. **12**, 12223 (2010).
[122] X. L. Ding, Y. X. Zhao, X. N. Wu, Z. C. Wang, J. B. Ma, and S. G. He, Chem. Eur. J. **16**, 11463 (2010).
[123] Z.-C. Wang, X.-N. Wu, Y.-X. Zhao, J.-B. Ma, X.-L. Ding, and S.-G. He, Chem. Eur. J. **17**, 3449 (2011).
[124] N. Dietl, R. F. Höckendorf, M. Schlangen, M. Lerch, M. K. Beyer, and H. Schwarz, Angew. Chem. Int. Ed. **50**, 1430 (2011).
[125] Z.-G. Zhang, H.-G. Xu, Y.-C. Zhao, and W.-J. Zheng, J. Chem. Phys. **133**, 154314 (2010).
[126] M. Nossler, R. Mitric, V. Bonacic-Koutecky, G. E. Johnson, E. C. Tyo, and A. W. Castleman, Jr., Angew. Chem. Int. Ed. **49**, 407 (2010).
[127] E. Janssens, S. M. Lang, M. Brummer, A. Niedziela, G. Santambrogio, K. R. Asmis, and J. Sauer, Phys. Chem. Chem. Phys. **14**, 14344 (2012).
[128] N. J. Mayhall, D. W. Rothgeb, E. Hossain, K. Raghavachari, and C. C. Jarrold, J. Chem. Phys. **130**, 124313 (2009).
[129] D. W. Rothgeb, E. Hossain, A. T. Kuo, J. L. Troyer, and C. C. Jarrold, J. Chem. Phys. **131**, 044310 (2009).
[130] J. E. Mann, D. W. Rothgeb, S. E. Waller, and C. C. Jarrold, J. Phys. Chem. A **114**, 11312 (2010).
[131] D. W. Rothgeb, E. Hossain, J. E. Mann, and C. C. Jarrold, J. Chem. Phys. **132**, 064302 (2010).
[132] D. W. Rothgeb, J. E. Mann, S. E. Waller, and C. C. Jarrold, J. Chem. Phys. **135**, 104312 (2011).
[133] J. E. Mann, S. E. Waller, and C. C. Jarrold, J. Chem. Phys. **137**, 044301 (2012).
[134] S. E. Waller, J. E. Mann, E. Hossain, M. Troyer, and C. C. Jarrold, J. Chem. Phys. **137**, 024302 (2012).
[135] S. E. Waller, J. E. Mann, D. W. Rothgeb, and C. C. Jarrold, J. Phys. Chem. A **116**, 9639 (2012).
[136] X. N. Wu, X. N. Li, X. L. Ding, and S. G. He, Angew. Chem. Int. Ed. **52**, 2444 (2013).
[137] X. N. Li, X. N. Wu, X. L. Ding, B. Xu, and S. G. He, Chem. Eur. J. **18**, 10998 (2012).
[138] N. Dietl, X. H. Zhang, C. van der Linde, M. K. Beyer, M. Schlangen, and H. Schwarz, Chem. Eur. J. **19**, 3017 (2013).
[139] N. Dietl, A. Troiani, M. Schlangen, O. Ursini, G. Angelini, Y. Apeloig, G. de Petris, and H. Schwarz, Chem. Eur. J. **19**, 6662 (2013).
[140] N. Dietl, M. Schlangen, and H. Schwarz, Angew. Chem. Int. Ed. **51**, 5544 (2012).
[141] J. B. Ma, Z. C. Wang, M. Schlangen, S. G. He, and H. Schwarz, Angew. Chem. Int. Ed. **52**, 1226 (2013).

[142]S. G. He, Y. Xie, Y. Guo, and E. R. Bernstein, J. Chem. Phys. **126**, 194315 (2007).
[143]S. G. He, Y. Xie, F. Dong, and E. R. Bernstein, J. Chem. Phys. **125**, 164306 (2006).
[144]M. J. Frisch, G. W. Trucks, H. B. Schlegel *et al.*, Gaussian 09, Revision C.01, Gaussian, Inc., Wallingford CT, 2009.
[145]A. D. Becke, Phys. Rev. A **38**, 3098 (1988).
[146]C. T. Lee, W. T. Yang, and R. G. Parr, Phys. Rev. B **37**, 785 (1988).
[147]A. D. Becke, J. Chem. Phys. **98**, 5648 (1993).
[148]W. Kohn and L. J. Sham, Phys. Rev. **140**, A1133 (1965).
[149]M. Dolg, H. Stoll, and H. Preuss, J. Chem. Phys. **90**, 1730 (1989).
[150]M. Dolg and H. Stoll, Theor. Chim. Acta **75**, 369 (1989).
[151]X. Y. Cao and M. Dolg, J. Chem. Phys. **115**, 7348 (2001).
[152]D. Andrae, U. Haussermann, M. Dolg, H. Stoll, and H. Preuss, Theor. Chim. Acta **77**, 123 (1990).
[153]A. Schafer, C. Huber, and R. Ahlrichs, J. Chem. Phys. **100**, 5829 (1994).
[154]H. B. Schlegel, J. Comput. Chem. **3**, 214 (1982).
[155]C. Peng, P. Y. Ayala, H. B. Schlegel, and M. J. Frisch, J. Comput. Chem. **17**, 49 (1996).
[156]C. Gonzalez and H. B. Schlegel, J. Phys. Chem. **94**, 5523 (1990).
[157]C. Gonzalez and H. B. Schlegel, J. Chem. Phys. **90**, 2154 (1989).
[158]D. G. Truhlar and M. S. Gordon, Science **249**, 491 (1990).
[159]S. R. Desai, H. B. Wu, C. M. Rohlfing, and L. S. Wang, J. Chem. Phys. **106**, 1309 (1997).
[160]G. E. Johnson, N. M. Reilly, and A. W. Castleman, Jr., Int. J. Mass. Spectrom. **280**, 93 (2009).
[161]C. Bürgel, N. M. Reilly, G. E. Johnson, R. Mitrić, M. L. Kimble, A. W. Castleman, Jr., and V. Bonačić-Koutecký, J. Am. Chem. Soc. **130**, 1694 (2008).
[162]L. H. Tian, T. M. Ma, X. N. Li, and S. G. He, Dalton Trans. **42**, 11205 (2013).